9

Imaging the Dynamics of Mammalian Neocortical Population Activity In Vivo

Amiram Grinvald, David Omer, Shmuel Naaman, and Dahlia Sharon

9.1 INTRODUCTION

The activity of highly distributed neural networks is thought to underlie sensory processing, motor coordination, and higher brain functions. These intricate networks are composed of large numbers of individual neurons, which interact through synaptic connections in complex, dynamically regulated spatiotemporal patterns. To understand the network properties and functions, it is helpful to study the ensemble activity of neuronal populations because coherent activity of many neurons, rather than individual cells, is often responsible for performing the function. Functionally related sub-networks of neurons are often spatially segregated, making imaging techniques ideal for monitoring population activity. Our understanding of the contribution of single neurons for generating percepts and controlling behavior can be improved within the context of the relationship between individual-level and population-level activity (see Chap. 10).

The remarkable performance of the mammalian brain arises from computations taking place in the neocortex. The neocortex is organized into cortical columns (Mountcastle 1957; Hubel and Wiesel 1962), which have lateral dimensions of a few hundred microns. Interactions within and between cortical columns occur on the time scale of milliseconds. To follow neuronal computations at the fundamental level of cortical columns in real-time therefore requires a spatial resolution of ~100 μm and a temporal resolution of ~1 ms. In vivo Voltage-Sensitive Dye Imaging (VSDI) (Grinvald et al. 1984; Orbach et al. 1985) fulfils these technical requirements and should help resolve many fundamental questions.

Electrical communication in cortical networks comprises two basic signals: subthreshold potentials (reflecting synaptic input onto dendrites) and suprathreshold action potentials (forming the neuronal output). VSDI appears to relate primarily to spatiotemporal patterns of the subthreshold synaptically driven membrane potentials simply because of the relatively larger area of neocortical dendrites. Therefore, VSDI allows monitoring the fluctuations of the membrane potential of the population away from and towards the threshold for action potential. Single unit and multi-unit recordings cannot monitor this activity, reflecting only spiking activity. The local field potential, which does reflect synaptic potentials, changes its polarity depending on the activity source and therefore provides ambiguous information about the sign of recorded activity (inhibition versus excitation). Furthermore, its spatial resolution is far lower. Therefore VSDI has a unique place among available techniques for measuring neural activity.

Here we describe how in vivo VSDI (Grinvald et al. 1984; Shoham et al. 1999; Grinvald and Hildesheim 2004) can be applied to anesthetized mammals. Another chapter (Chap. 10) provides information on cortical spatiotemporal dynamics in awake subjects during behavior. We describe previous findings and technical advances, mostly from our lab, and how VSDI has been combined with intracortical microstimulation, single-unit recording, local-field-potential recording, and targeted injections. We conclude by discussing further technical developments to overcome current limitations.

9.2 PRINCIPLES OF VOLTAGE-SENSITIVE DYE IMAGING IN VIVO

VSDI in vivo is a form of functional optical imaging of neuronal activity that utilizes extrinsic fluorescence probes (see Chaps. 1 and 2) to monitor membrane potential changes in real-time. It thus differs from optical imaging based on intrinsic signals in two important ways. The first, its biggest advantage, is that it offers a millisecond temporal resolution without compromising spatial resolution. The second, its biggest disadvantage, is that it relies on minimally invasive staining of the cortex with vital voltage-sensitive dyes (VSDs).

To perform optical imaging of electrical activity in vivo, the preparation under study is first stained with a suitable VSD (Chaps. 1 and 2). The dye molecules bind to the external surface of excitable membranes and act as molecular transducers that transform changes in membrane potential into optical signals. These optical signals are observed as changes in absorption or emitted fluorescence, and respond to membrane potential changes in microseconds (Chap. 1). The amplitude of the VSD signal varies linearly with both the membrane potential changes and the membrane area of the stained neuronal elements (Chap. 1). These optical changes are monitored with light imaging devices positioned in a microscope image plane. Optical signals using VSDs were first recorded by Tasaki et al. (1968) in the squid giant axon and by Salzberg et al. (1973) in the leech ganglia. In vivo experiments in rat visual cortex began in 1982 (Grinvald, Orbach and Cohen, unpublished results) and revealed several complications that had to be overcome. One complication was the large amount of

Amiram Grinvald, David Omer, Shmuel Naaman and Dahlia Sharon • Department of Neurobiology, Weizmann Institute of Science, Rehovot 76100, PO Box 26, Israel
Dahlia Sharon • Department of Psychology, Stanford University, Stanford, CA 94305, USA

M. Canepari and D. Zecevic (eds.), *Membrane Potential Imaging in the Nervous System: Methods and Applications*,
DOI 10.1007/978-1-4419-6558-5_9, © Springer Science+Business Media, LLC 2010

noise caused by respiratory and heartbeat pulsations. In addition, the relative opacity and packing density of the cortex limited the penetration of the excitation light and the ability of dyes to stain deep layers of the cortex. Subsequently, new, improved dyes that overcame these problems were developed (e.g., RH-414) and an effective remedy for the heartbeat and respiratory noise was found by synchronizing data acquisition and the respiration with the electrocardiogram and subtracting a no-stimulus trial. These improvements facilitated the in vivo imaging of several different sensory systems, including the retinotopic responses in the frog optic tectum (Grinvald et al. 1984), and the whisker barrels in rat somatosensory cortex (Orbach et al. 1985), and experiments in the salamander olfactory bulb (Orbach and Cohen 1983). The development of more hydrophilic dyes improved the quality of the results obtained in cat and monkey visual cortex (e.g., RH-704 and RH-795, Grinvald et al. 1994).

The newest generation of VSDs, introduced in the late 1990s, offers a 30-fold improvement in signal-to-noise ratio over the above-mentioned early dyes. This was accomplished by designing oxonol dyes, which are excited outside the absorption band of hemoglobin, thus minimizing pulsation and hemodynamic noise (Fig. 9.1). With this advance it has become possible to reveal the dynamics of cortical information processing and its underlying functional architecture at the necessary spatial and temporal resolution in both anesthetized and behaving animals. Furthermore, it finally became possible to obtain good signals without trial averaging, thus facilitating the exploration of neocortical dynamics including spontaneous on-going activity. Additional advances related to the implantation of transparent artificial dura by Arieli et al. (2002) now allow chronic recordings to be taken over a long period of time (Chap. 10). Optical imaging has also been performed simultaneously with intracellular recording, extracellular recording, microstimulation, and tracer injection due to the development of an electrode assembly attached to a cranial window (Arieli and Grinvald 2002).

9.2.1 Relationship Between Voltage-Sensitive Dye Signals and Intracellular Recordings In Vivo

In simple preparations, when single cells or their processes can be visualized, the dye signal looks just like an intracellular recording. Controversies about what the dye signal reflects during in vivo measurements were resolved by combining VSDI with intracellular recordings in vivo, first in cat visual cortex (Sterkin et al. 1998; Grinvald et al. 1999) and in the rat somatosensory cortex (Petersen et al. 2003a). The results established that the dye signal precisely reports changes in membrane potential (red and green traces in Fig. 9.2A, red and yellow in Fig. 9.2B and red and black in Fig. 9.2C–F). The tight correlation between the intracellular neuronal recording and the VSD signal also indicates that the contribution of slow glial depolarization to the VSD signal is minimal. The linearity is shown in Fig. 9.2F.

During in vivo imaging of the neocortex, a single pixel contains the blurred images of various neuronal compartments – including the dendrites, axons, and somata of a population of neurons – rather than a single cell. The VSD signal is linearly related to the stained membrane area, and most of the dye signal originates from cortical dendrites and non-myelinated axons rather than cell bodies, because their membrane areas are orders of magnitude larger than that of neuronal somata or confined non-myelinated axons. The dendrites of cortical cells are often far more confined than the axons, so most of the signals in a given pixel originate from the dendrites of nearby cortical cells. Therefore, the existence of a dye signal in a particular cortical site does not necessarily imply that cortical neurons at that site are generating action potentials. However, the peak/s of the VSD

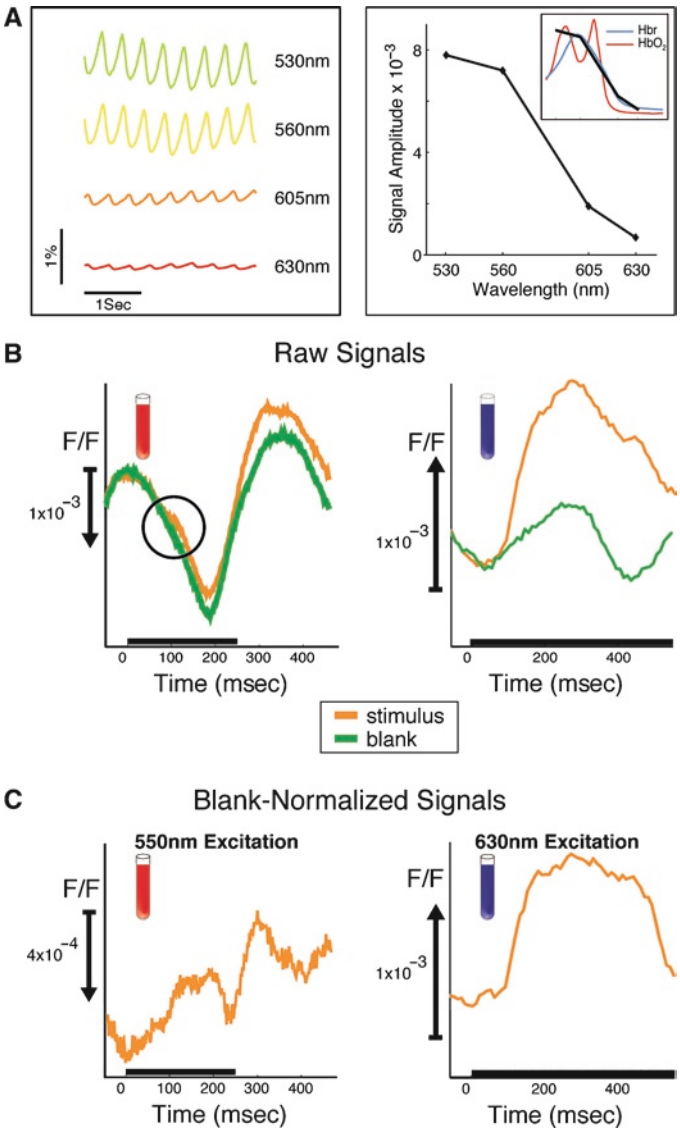

FIGURE 9.1. "Blue dyes": Thirtyfold improvement in the signal-to-noise ratio. (A) Wavelength dependency of heart-beat and respiration signals. The *left panel* illustrates optical reflectance signals from cat visual cortex measured at several wavelengths. The color of the line schematically represents the wavelength of the illuminating light. The signals were averaged over the entire imaged area. The *right panel* plots the peak to peak amplitude as a function of wavelength, illustrating the fall off with increasing wavelength in this range. The inset shows the amplitude plot (normalized) on the same axes as the textbook absorption of oxy- and deoxy-hemoglobin, illustrating the close relationship between the two. (B) Time course of the evoked voltage-sensitive dye signals. The left and right top panels illustrate the signals from different experiments using the red dye RH-795 and the blue dye RH-1692, respectively. The curves show the raw fluorescence signals, without subtracting the blank, integrated over the imaged area (cat visual area 18) and averaged over trials. The *orange curves* are from the stimulated condition and the *green* lines are the blank data (no stimulus). Data acquisition was synchronized to the heart-beat. The *solid black line* marks the stimulus period. The *circle* in the left panel (RH-795) points to the time of the fast evoked signal showing its minute magnitude relative to the heartbeat signal. Note the large amplitude of the evoked signal relative to the heart-beat signal for the *blue dye* (right). This is true despite the larger total raw signal for the red dye. Note also that the sign of the heartbeat signals from the two dyes are opposite. (C) The same data as (B) but with the heart-beat signal removed by subtracting the blank condition. Note the large heart-beat artifact with the red dye at the time of the second heart-beat. Again the blue dye produces much better signal-to-noise ratio, allowing examination of small components in the response and longer recording interval that are still reliable. In both cases 16 presentations were averaged.

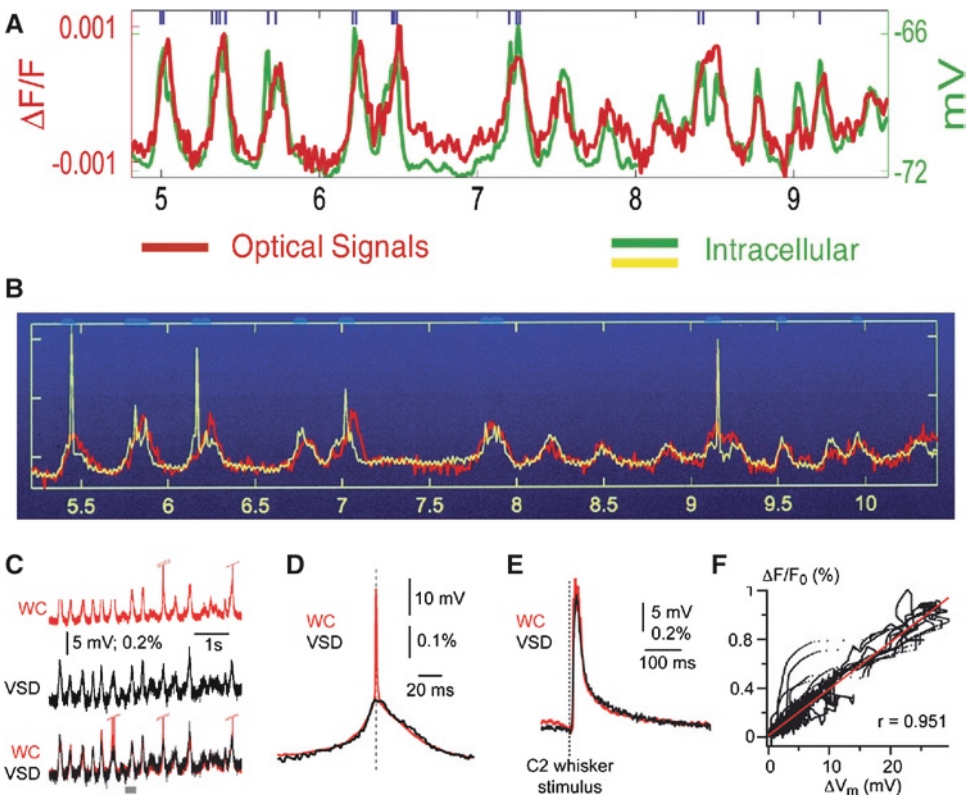

FIGURE 9.2. The similarity between the cortical dye signal in vivo from a small population of neurons and intracellular recording. (A) Two traces showing simultaneous intracellular and optical recording for 5 s, performed in a deeply anesthetized cat, a condition in which spontaneous changes in membrane potential are highly synchronized in a large population of neuron. The intracellular recording is depicted by the *green* trace and the population signal by the *red* trace. The action potentials were truncated and occurred at times marked by the *short blue lines* at the top. (B) The intracellular recording is depicted by the *yellow trace*. The action potentials were not truncated. One can see that the optical signal from the population next to the electrode is not picking up action potentials, presumably because the membrane area of the dendrites monitored by a single pixel is much larger than the membrane area of the non-myelinated axons originating from that cell (the action potentials are not synchronized whereas the synaptic potentials are). (A, B) modified from Sterkin et al. (1998). (C) Similar simultaneous recording from the rat somatosensory cortex showing once again that the population signal is similar to the synaptic potential but not to the action potential. *WC* whole cell recordings. (D) Same but on an expanded time scale, showing the resemblance between the dye signal and the intracellular recording. (E) Simultaneous recordings of an evoked response resulting from sensory stimulation of moving whisker C2. (F) The linearity of the Dye signal versus the membrane potential change. (C–F) modified from Petersen et al. (2003b).

response to a suprathreshold stimulus corresponds to the spiking zone, which is to be expected from the fact that synaptic activity peaks in this zone too (Jancke et al. 2004; Sharon et al. 2007). In vivo the VSD signal thus reflects mainly dendritic activity, making VSDI optimal for exploring population dynamics of local subthreshold neuronal activity. However, the VSD signal also contains some spiking information (output), which remains to be exploited.

9.2.2 Imaging from the Mammalian Brain In Vivo

A major technical impediment to imaging anesthetized or awake animals is movement of the brain. A critical aspect of imaging neocortical activity in vivo is therefore to obtain a stable view of the cortex. The obvious solution is to fix the head relative to the imaging apparatus as done for electrical or intracellular recordings. Head-fixation bars can be attached to the skull of the animal. Next, a sealed recording chamber should be used to minimize brain pulsations relative to the skull. A tandem-lens macroscope (Ratzlaff and Grinvald 1991) can then be mounted in a stable location relative to the fixed head position for epifluorescent VSDI with suitable illumination and camera equipment. For a picture of the imaging set up see Fig. 10.1 in Chap. 10.

9.2.3 Spatial and Temporal Resolution

As already mentioned, VSDs respond to membrane potential changes in microseconds at a spatial resolution of ~0.5 μm. However, the practical spatiotemporal resolution that can be obtained by in vivo imaging depends on factors other than the resolution of the dye molecule's response, such as light scattering within the imaged tissue, photodynamic damage, and optics of the data acquisition apparatus including the detector resolution. Below we discuss some of these factors. Empirically, we find that current dyes and equipment allow excellent signal-to-noise at a sampling rate of 100–200 Hz with each pixel looking at a 50 × 50-μm area of cortex. Light scattering is a major determinant of spatial resolution, and photodynamic damage is an important determinant of signal-to-noise ratio, both spatially and temporally because it limits the light intensity used to reduce shot noise or the extent of signal averaging used to improve the signal-to-noise ratio.

Additional concerns include limited depth of penetration into the cortex, and possible pharmacological side effects. The new oxonol dyes have largely alleviated the problems of pharmacological side-effects and photodynamic damage. First, intracellular recordings in vivo have directly confirmed that stained cortical cells maintain their response properties (Ferster, Lampl, Arieli and Grinvald, unpublished results). Furthermore, long-term VSDI in awake

monkeys have indicated that, even after a year of imaging, monkey visual cortex continued to function normally: the animal maintained normal performance in tasks that required the normal functioning of the cortical area which was repeatedly imaged for up to a year.

The primarily dendritic origin of the VSD signal (see above) also affects the spatial resolution of VSDI, because the dendrites of cells in a given cortical column typically cross cortical areas that correspond to adjacent cortical columns, which have different functional properties. Therefore, the dendritic view of activity offered by VSDI is in effect somewhat blurred relative to the somatic activity. Differential imaging provides some remedy to this problem as well as the light scattering problem. Using differential imaging whenever applicable may provide even 1-μm resolution and depends mostly on the signal-to-noise ratio which can be obtained.

Improvements in the dyes and in the spatial resolution of fast cameras have thus made it possible to obtain high resolution functional maps of somatosensory whisker barrels, olfactory glomeruli and visual orientation columns, "lighting up" in milliseconds with a signal-to-noise ratio even better than that obtained with the slow intrinsic signals. Additional developments will undoubtedly introduce further improvement.

9.2.4 Long-Term Repeated VSDI

To facilitate repeated imaging sessions, the resected dura matter is substituted with artificial dura mater. A careful cleaning procedure has allowed repeated VSDI sessions in monkeys two to three times a week over a period longer than a year (Arieli et al. 2002). This topic is described in more detail in Chap. 10. Long-term imaging allows exciting new type of experiments related to development, plasticity, learning and memory, and recovery after trauma or stroke.

9.2.5 Integrating VSDI with Electrode Techniques

VSDI can easily be combined with standard electrode-based techniques. Whereas optimal mechanical stability for imaging is provided by sealed cranial windows, these do not allow electrodes to be introduced. One approach is to cover the cortical surface with agarose and stabilize it by a cover slip. A small gap between the edge of the cover slip and the wall of the recording chamber allows oblique entry of electrodes into the rodent cortex (Petersen et al. 2003a, b; Berger et al. 2007; Ferezou et al. 2006, 2007). For cats and monkeys a sliding-top cranial window was developed with a removable microdrive-positioned electrode (Arieli and Grinvald 2002). VSDI can then be combined with microstimulation, extracellular recording (single- and multiple-unit recording and local field potential), intracellular recording, patch recordings and targeted injection of tracers. Recordings can either be made simultaneously and/or can be targeted to specific regions based on the functional imaging data. (Arieli and Grinvald 2002)

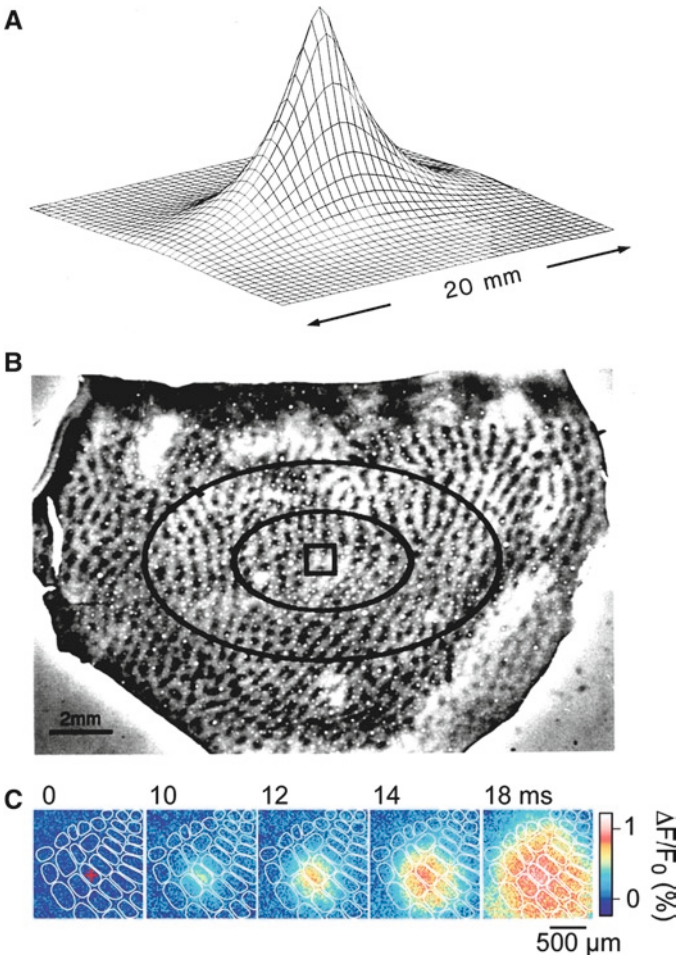

FIGURE 9.3. Many functional domains are activated during the processing of a small retinal image or a single whisker. (A) Calculation of the activity spread from a small patch in layer 4 (a 1 × 1 mm square) within the upper cortical layers of a macaque. This cortical activation was produced by a retinal image of approximately 0.50 × 0.25° that was presented to both eyes. The "space constants" for the exponential-activity-spread measured with the dye experiments were 1.5 and 2.9 mm in the cortical axes perpendicular and parallel to the vertical meridian representation, respectively. (B) Direct activation in layer 4 (of the area within the square; calculated from retinotopic extracellular recordings) and the spread in layers 2/3 (elliptical contours; calculated from VSDI) are shown superimposed on a histological section showing the mosaics of cytochrome oxidase blobs, close to the border between cortical areas V1 and V2. The center ellipse shows the contour at which the amplitude of cortical activity drops to 37% of its peak. The larger ellipse shows the contour at which the spread amplitude drops to 14%. More than 10,000,000 neurons reside in the cortical area bounded by the large ellipse containing a regular mosaic of about 250 blobs. Adapted from Grinvald et al. (1994) with permission from the Society for Neuroscience. (C) The exact spatio-temporal pattern of the spread in the somato-sensory cortex in response to a single barrel stimulation. The temporal resolution was 2 msec/frame. Modified from Petersen et al. (2003b) and from Ferezou et al. (2006).

9.3 EXPLORATIONS OF POPULATION DYNAMICS IN VISUAL CORTEX

9.3.1 Lateral Extent of Focal Activation and the Lateral Spread Dynamics

Retinotopic VSDI experiments in monkey have been used to investigate how far across the cortical surface synaptic activation spreads from a sensory point stimulus – the cortical point-spread function (Fig. 9.3A). Activity spreads over a cortical area much larger than predicted on the basis of standard retinotopic measurements in layer 4, but is consistent both with the anatomical finding of long-range horizontal connections in visual cortex and with intracellular recordings. The cortical point spread function was calculated from these experiments and projected onto a histological section of cytochrome oxidase blobs (Fig. 9.3B) to show its relationship to individual cortical modules.

The stimulus caused spiking activity only in neurons in the marked small square, which contains four cortical modules. However, more than 250 blobs had access to the information carried by the signal spread, at a signal amplitude of at least $1/e^2$ of

maximum. The apparent space constant (signal decrement to 1/*e* of peak) for the spread was 1.5 mm along the cortical axis parallel to the ocular dominance (OD) columns, and 3 mm along the perpendicular axis. The spread velocity was 0.1–0.2 m/s. Much higher spatial resolution data showing similar spread in the somatosensory cortex has been first reported by Petersen and collegues (Petersen et al. 2003a, b; Fig. 9.3C) and several subsequent papers from the same group.

These results indicate extensive distributed processing, and were further investigated also in cat visual cortex with the new generation of dyes and an imaging system offering subcolumnar resolution, taking a more detailed look at the "inverse" of the receptive field – the region of cortical space whose spatiotemporal pattern of electrical activity is influenced by a given sensory stimulus. The spatiotemporal properties of this activated area, which we refer to as the cortical response field, were studied using VSDI for responses to small, local drifting oriented gratings. One might expect a smooth decline in activity level from the cortical response field peak to periphery, as the overlap between the stimulus and the aggregate receptive field at each cortical location decreases. However, this is not the case, and as shown in Fig. 9.4A, the average cortical response field during a late time window (~140–515 ms after stimulus onset) has a distinctive spatial structure: an initial rapid drop from the peak is followed by a slower-sloped region, the plateau, beyond the rim of which (black contour line) a rapid decline in activity level occurs in the periphery. Plateau rim location was largely independent of stimulus orientation (Fig. 9.4B). The task of obtaining single-condition responses to these small stimuli at 10-ms resolution, especially demanding during early activation when response amplitude is low, was undertaken to determine the dynamics and significance of this spatial structure.

Results show that initially the response consists of a flat-topped plateau (Fig. 9.4C, 40 ms), and that the peak emerges upon it only about 20 ms later (Fig. 9.4C, 60 ms). See also Movie 9.2. The peak region amplifies relative to plateau amplitude for an average of 25 ms, and after this time only the plateau's height above the periphery

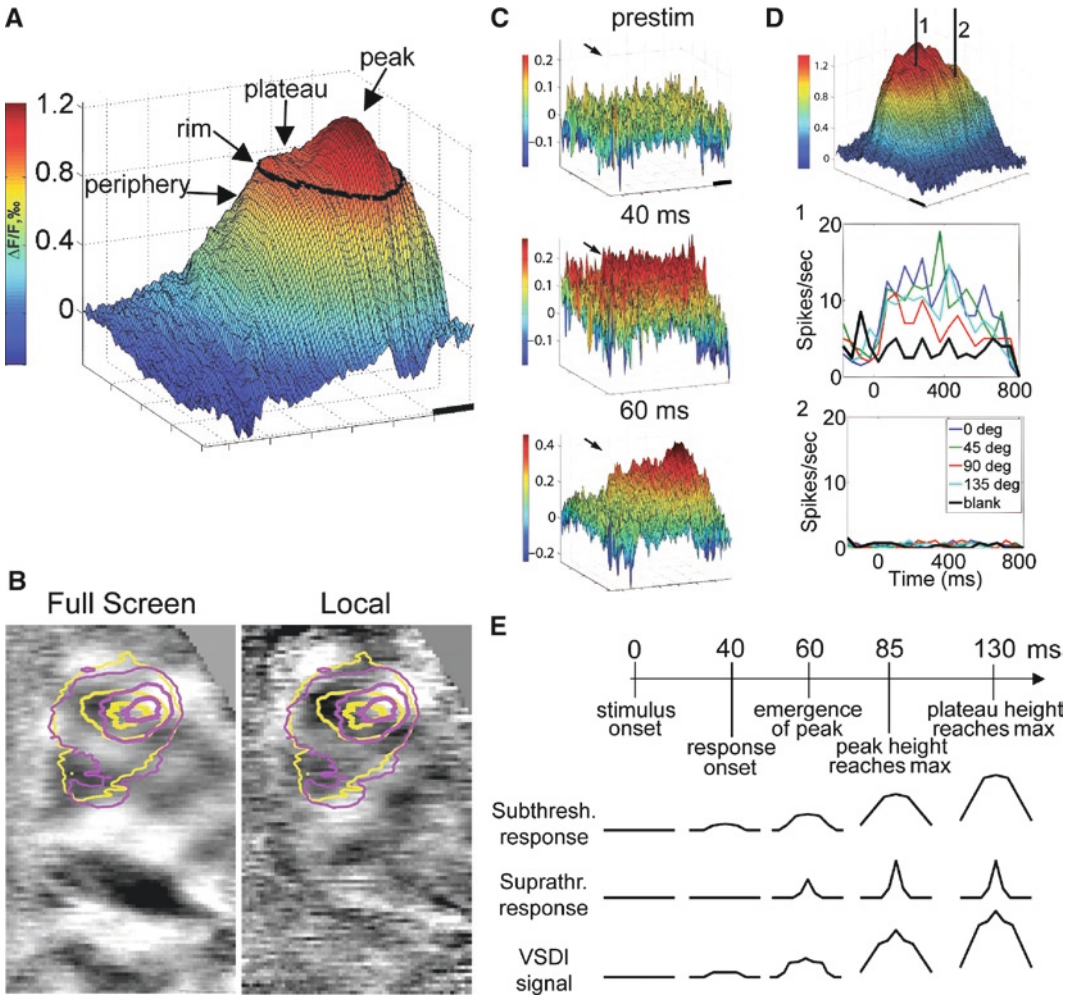

FIGURE 9.4. Cortical response fields in response to local visual stimuli: structure and dynamics. (A) The cortical response field averaged over 140–515 ms after presentation of a local drifting grating exhibits the characteristic plateau + peak spatial structure. Beyond plateau rim, responses in the periphery decay quickly. (B) Relationship between response field to local grating stimuli of two orthogonal orientations (*yellow* and *magenta contour lines*) and differential orientation map from full-screen (*left*) and local (*right*) stimuli. Plateau rim (*outer contour lines*) is similar among the two orientations, whereas the peak zone (*inner contour lines*) corresponds better to the underlying orientation map. (C) Early dynamics: the initial response (40 ms) is a flat-topped plateau, with the peak emerging upon it only later (60 ms). (D) Spiking is restricted to the peak zone. (*Top*) A cortical response field with the locations of two extracellular electrodes. (*Middle*) Spiking responses are evoked in the peak zone (location 1) by the local stimulus. (*Bottom*) Spiking is absent in response to the same stimulus in the plateau away from the peak (location 2). (E) Timeline of the population response (*top*) and the proposed underlying subthreshold and suprathreshold responses (*middle*). The VSDI signal (*bottom*) is a sum of these two components, with the subthreshold response contributing a larger component due to relative membrane areas.

continued to increase, reaching a maximum at 130 ms. The qualitatively different response dynamics suggested to us that spiking activity may be restricted to the peak zone, and that despite the high amplitude VSD signal at the plateau, neurons are not spiking. Extracellular recording showed that indeed spiking is evoked in the peak zone, but not at the plateau (Fig. 9.4D). These results can be explained by a simple model which views the VSD signal as a weighted sum of all membrane potential changes: subthreshold responses and suprathreshold responses, with the former supplying the larger contribution to the signal due the larger membrane area involved (Fig. 9.4E). The subthreshold response is wider in spatial extent because subthreshold receptive fields are larger than suprathreshold receptive fields. In this model, the sharp drop in activity occurring at the rim of the plateau and beyond is a result of reaching the edge of the area where neurons' subthreshold receptive field fully contains the stimulus. Smaller decrements are exhibited as long as the stimulus is fully contained within neurons' receptive field, i.e., within plateau rim.

The view that arises from these results is that, while unsurprisingly spiking activity occurs only for neurons with receptive fields at the correct location and orientation, a near-maximal subthreshold response is evoked in an area spanning several square millimeters, plunging quickly only once subthreshold receptive field overlap with the stimulus starts to decrease. Plateau activation to just below spiking threshold thus encompasses all orientations in an area representing a region of visual space larger than the stimulus. This interesting neuronal strategy primes the cortex for processing of subsequent stimuli, and could be involved in stimulus-driven attentional capture and in motion processing.

9.3.2 Dynamics of Shape Processing

Although orientation selectivity in the visual cortex has been explored for decades, the question of the interplay between feedforward processes and intracortical connections underlying this property has remained open. Two families of mechanisms have been proposed to play a role in the emergence of the highly orientation-selective responses of cortical visual neurons, a property not shared by their thalamic inputs. Feedforward-only models suggest appropriate alignment of thalamic input as the mechanism, whereas recurrent models suggest that intracortical interactions are more important. The response dynamics in visual cortex are fundamental to answering this question, because the feedforward explanation predicts that orientation selectivity should remain constant with time from stimulus onset, whereas if recurrent interactions are important then selectivity should change as the cortical network performs its processing. Traditional electrophysiological techniques have not been able to give a conclusive result regarding this issue. VSDI is ideally suited to resolve it, being a high spatiotemporal resolution population imaging technique that emphasizes synaptic input.

To investigate the dynamics of orientation selectivity, high-quality single-condition maps were obtained in cat visual cortex. A time-series of the initial response is shown in Fig. 9.5A for two orthogonal orientations. As soon as the response can be observed (30–40 ms), the two orthogonal stimuli preferentially activate complementary patches of cortex, seen in the differential map (Fig. 9.5B).

The modulation depth, i.e., the amplitude of the difference between the responses to the two stimuli, increases at the beginning of the response, and peaks at about 100 ms (Fig. 9.5C). In order to calculate orientation tuning curves, however, differential maps and time-courses are of no use, and single-condition responses to several orientations are needed. Single-condition maps at different latencies are shown in Fig. 9.5A for two orientations, whereas Fig. 9.5D (top) shows single-condition timecourses averaged over the imaged pixels. The average evoked response to the preferred and orthogonal stimuli are plotted (blue and yellow, respectively). The tuning curve at each time point was calculated from the single-condition responses corresponding to the six different orientations presented (Fig. 9.5E). The immediate impression is that of tuning curves with a constant shape but changing amplitude. The map of preferred orientation does not change as time from stimulus onset progresses, as shown in Fig. 9.5F and in Movie 9.1 (available at http://www.weizmann.ac.il/brain/grinvald/html/movie_galley.html, Movie 3). Indeed, the half-width at half height of tuning curves, as well as preferred orientation, were steady right from response onset (30–40 ms after stimulus onset). Therefore, sustained intracortical processing does not seem to be necessary – at least for most neurons – to determine orientation tuning width and preferred orientation.

Other aspects of the response also affect orientation selectivity. The modulation depth of the response changes over time, decreasing after a peak at 100 ms (Fig. 9.5C). An intriguing phenomenon is nearly undetectable in the differential time-course, but becomes obvious when considering the evoked single-condition responses (Fig. 9.5D). Between 50 and 80 ms after stimulus onset, there is a notch (Fig. 9.5D) in the evoked response, equivalent to a deceleration followed by acceleration in the rise-time – this is termed the "evoked DA notch" (deceleration–acceleration). Furthermore, the evoked DA notch is more pronounced in response to the orthogonal stimulus than to the preferred (Fig. 9.5D). Shunting inhibition peaks at about 70 ms in cat area 17 (Bringuier et al. 1998), and could be the suppressive mechanism underlying the DA notch. These response properties – the increase and subsequent decrease of modulation depth (dynamic amplification of the orientation-selective response component), the existence of the DA notch and its orientation-selectivity – are difficult to explain based on properties of the thalamic input.

These results suggest that thalamic input may be the major determinant of orientation tuning width for most cortical neurons, but that intracortical processing is critical in amplifying the orientation selective component of the response. They also suggest that intracortical suppression contributes to this process by preventing the orthogonal response from increasing as rapidly as the response to the preferred orientation.

9.3.3 Long-Range Horizontal Spread of Orientation Selectivity Is Controlled by Intracortical Cooperativity

During the last three decades, the intra-cortical anatomical connectivity made by the horizontal connections has been extensively explored in multiple species. It has generally been concluded that horizontal axons in visual cortex bind distant columns sharing similar orientation preference. However, the functional selectivity of the horizontal spread has never been measured directly. One reason is that the connections made by the horizontal axons are difficult to record since they only have a subthreshold impact on their post-synaptic targets. Therefore, to unveil the functional expression of the horizontal connectivity, it is mandatory to have access to the activation of the horizontal network at the subthreshold, postsynaptic integration, level (Chavane et al. 2010) reported a multi-scale analysis of visually driven horizontal network activation, using direct population and intracellular measures of post-synaptic integration. VSDI shows that while global activation in response to a local stimulus exhibits long-range horizontal spread (Fig. 9.6A, F), the orientation-selective component of this response does not spread beyond the feedforward

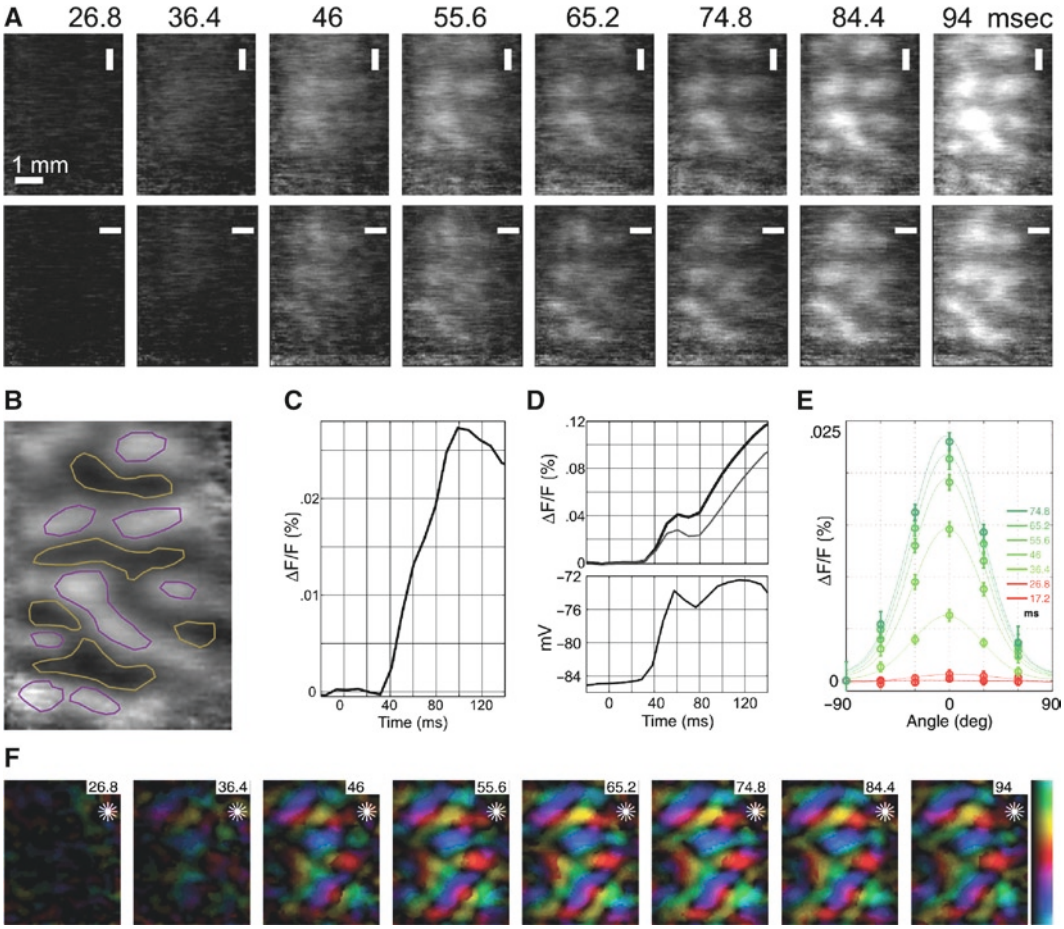

FIGURE 9.5. Width of the orientation tuning curve is constant, but its amplitude increases dynamically during the first 40–60 ms of the response. (A) Time-series of single-condition orientation maps in cat produced in response to two orthogonal visual stimuli (*top* and *bottom rows*). (B) Spatial pattern revealed by differential imaging. Neurons within the *yellow lines* are selective for vertical; *red* – horizontal. (C) Temporal pattern of differential activity. The evoked DA (deceleration–acceleration) notch is barely visible. (D) Top, time-course of the evoked response to preferred (*blue*) and orthogonal (*green*) orientations. The two responses have the same onset latency but the response to the preferred orientation is larger from the beginning. A striking feature of the evoked responses is the DA notch, confirmed with intracellular recordings (*bottom*). (E) Orientation tuning curves at different times after stimulus onset. The curves after response onset (*green*) have the same shape but different amplitudes. The baseline of the curves was shifted to facilitate comparison. (F) Time-series of orientation-preference "polar maps": color represents preferred orientation (top to bottom of color scale on right is 0–180°) and brightness represents the amplitude of differential response. Preferred orientation is steady from response onset. Adapted from Sharon and Grinvald (2002) with permission from the American Association for the Advancement of Science.

cortical imprint of the stimulus (Fig. 9.6C, H). Orientation selectivity decreases exponentially with horizontal distance. Therefore, beyond a distance of one hypercolumn, horizontal functional connectivity no longer obeys a binding rule preserving iso-orientation preference with this type of stimulus. Intracellular recordings show that this loss of orientation selectivity arises from the diversity of convergence patterns of intracortical synaptic input originating from beyond the classical receptive field.

In contrast, when increasing the spatial summation evoked by the stimulus – for example by presenting annular stimuli, orientation-selective activation spreads beyond the feedforward imprint (compare Fig. 9.7A, B: the orientation map). It was therefore concluded that stimulus-induced cooperativity at the network level is needed for the emergence of long-range orientation-selective spread.

This study shows two different dynamic behaviors of the same network for two distinct stimulus configurations: a single local stimulus does not propagate orientation preference through the long-range horizontal cortical connections, whereas stimulation imposing spatial summation and temporal coherence facilitates the build-up of propagating activity exhibiting a strong orientation preference. These observations do not necessarily contradict each other. They point to the possibility that complex stimulus configurations are allowed and expected based on activation within a locally confined region in visual space, whereas an iso-oriented stimulus with a large spatial extent supports the expectation of that specific orientation throughout a yet-larger area.

9.3.4 Dynamics of Transitions Between Different Cortical Representations of Visual Inputs

The previous series of experiments dealt with questions regarding the representation of a single stimulus. In a different series of experiment, Na'aman and Grinvald set out to characterize the temporal transition between stimulus representations. In one example switches between full-field oriented gratings were studied, with different conditioning stimuli presented for 500 ms followed by a constant test stimulus (Fig. 9.8). Transitions between representation pairs took 30–100 ms, depending on the spatial

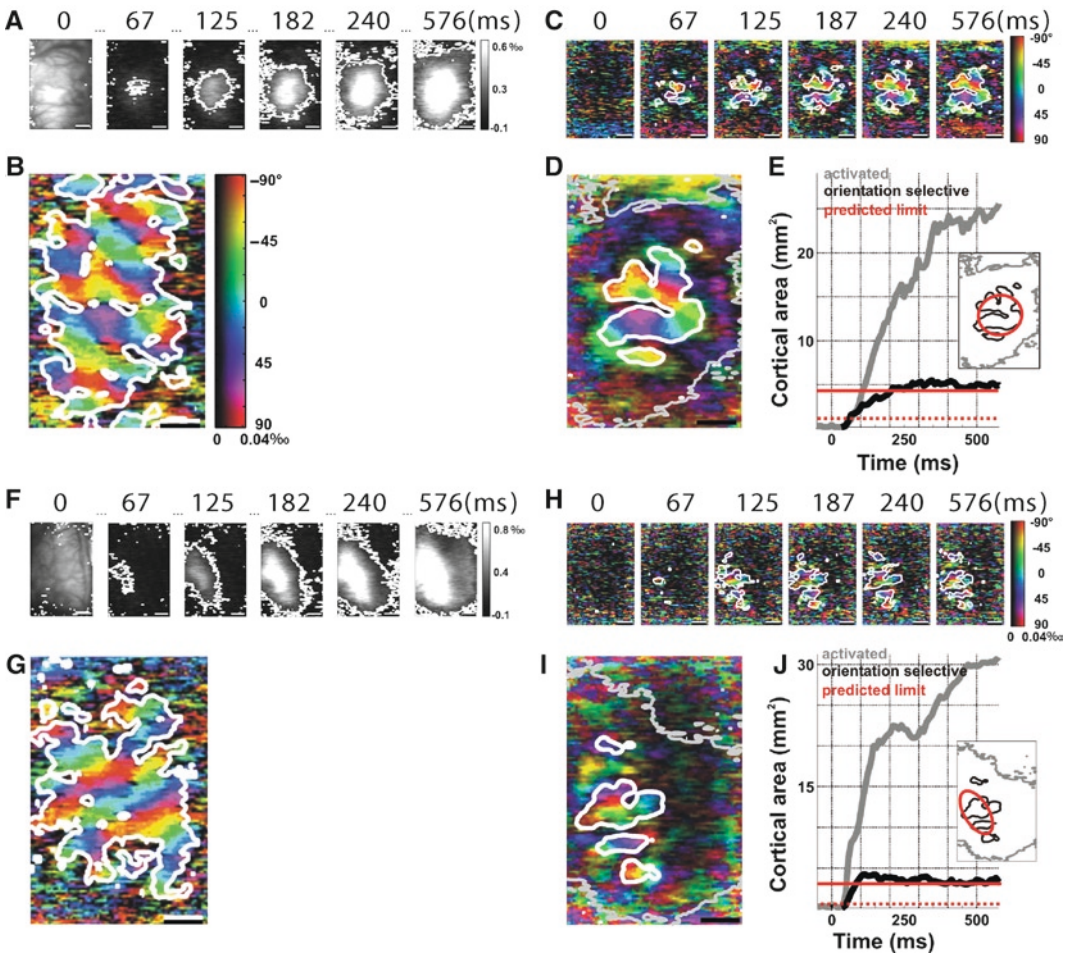

FIGURE 9.6. the horizontal spread away from the feedforward imprint is loosing its orientation tuning. (A, F) Time-series of the cortical response propagation evoked by a local stimulus (averaged over four orientations). (A) is an example from area 17 (stimulus diameter 2°; eccentricity of 4.1°; average of 28 trials) and (F) is from area 18 (stimulus diameter 4°; eccentricity of 7.6°; average of 32 trials). The imaged cortical area is shown in the first frame. (B, G) the polar maps obtained with full field stimulation using all orientations. Color hue and brightness code respectively for the preferred orientation and the strength of the orientation bias. (C, H) and (D, I) Polar maps of the orientation tuning in response to the local small stimulus (C, H time series D, I polar maps at late times). The white contour delineates the region significantly activated (E, J) superimposition over the late activation map is the feedforward imprint (red ellipse) limit of the stimulus.

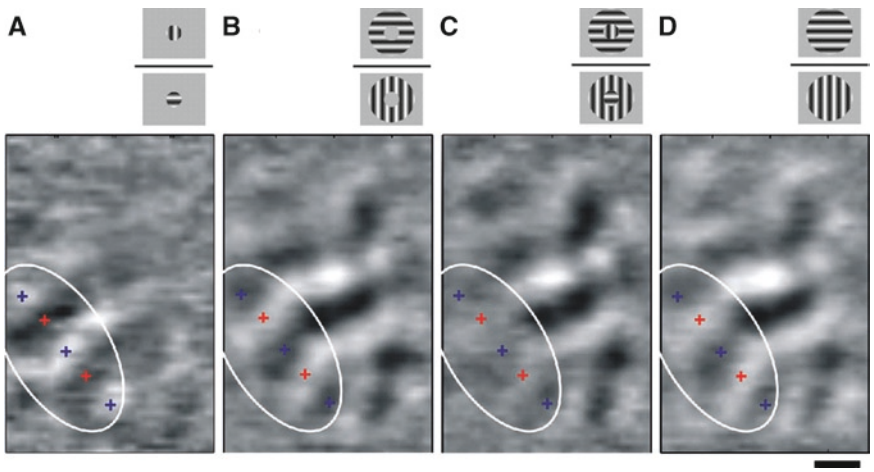

FIGURE 9.7. Horizontal spread and center-surround competition. (A) Area 18 differential map obtained by dividing the responses to horizontal versus vertical gratings presented through a central disk aperture (stimulus diameter 4° at an eccentricity of 7.6°; see cartoons). Orientation map is confined locally. (B) In comparison, displaying a larger grating through an annular aperture without stimulating the central disk (stimulus inner diameter, 4°, outer diameter, 12°, same eccentricity) results in the propagation of an oriented-selective signal within the cortical representation of the central disk region. (C) When both stimuli compete in a composite cross-oriented configuration, the orientation map disappears within the retinotopic representation of the central disk. (D) Control condition with iso-oriented center-surround configurations. The white contour encircles the expected retinotopic representation of the central disk. Scale bar is 1 mm.

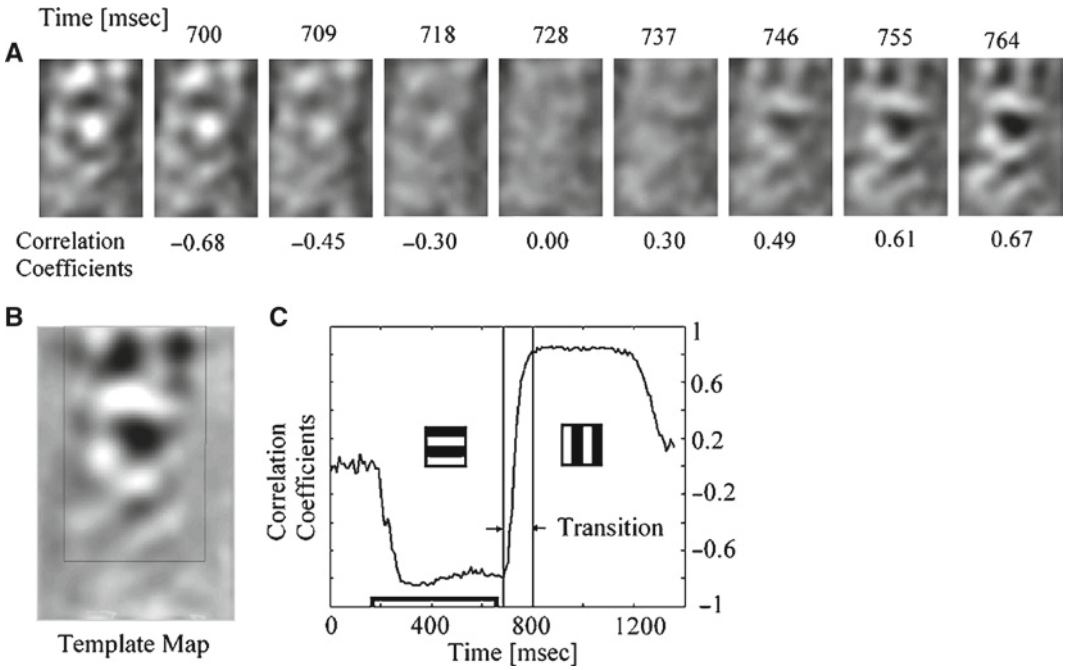

FIGURE 9.8. Quantifications of the transition dynamics. (A) shows the differential orientation maps dynamics just before, during and after transition. The acquisition time of each frame is 9.1 (ms) shown at the top, Here time 0 is defined as start of data acquisition. Correlation coefficient values of each frame with the template map (B) appear at the bottom of each frame. (B) the average response to the test stimuli the square gray region used as the template map. (C) Correlation coefficients as a function of time calculated between the template map to each frame during the presentation of the conditioning and the test stimuli. These data represent and average of 32 repetitions.

frequency, drift velocity, orientation, and contrast of the two stimuli. Additional details are still unpublished.

9.3.5 Neural Mechanisms of the Line-Motion Illusion

In another experiment we explored a temporal transition between two stimuli that gives rise to a visual illusion. The illusion of motion that can be produced by transition between two non-moving stimuli was described almost a century ago by Gestalt psychologists. In one variant of this phenomenon, the "line-motion" illusion, motion perception can be induced by a stationary square immediately followed by a long, stationary bar. The percept is that of the bar "sweeping" away from the square (Fig. 9.8A). The neuronal underpinnings of this illusion remain unknown, and VSDI was used to explore the associated subthreshold responses, combined with extracellular recordings to monitor spiking responses. We tested the hypothesis that the preceding square sets up a subthreshold activity gradient, such that when the stationary bar appears its response is superimposed on the preceding gradient, resulting in an increasing delay for reaching spike threshold with distance from the representation of the square stimulus.

The responses of anesthetized cat visual cortex to five stimuli were imaged using VSDI: a stationary small square; a stationary long bar; a moving square; a drawn-out bar; and the line-motion. Flashing the bar alone evoked the expected localized, short-latency and high-amplitude activity patterns (Fig. 9.9B second row). Three regions of interest (ROIs) were defined (Fig. 9.9C), and responses to the bar alone simultaneously crossed threshold at all three ROIs (Fig. 9.9D, black traces). However, presenting a square 60–100 ms before the bar (line-motion stimulus) induced dynamic activity patterns (Fig. 9.9B fourth row), which resembled those produced by fast movement (Fig. 9.9B third row). ROI timecourses confirmed that a critical threshold VSD signal amplitude was reached at successive times for the line-motion stimulus (Fig. 9.9D, blue traces). The spatiotemporal activity gradient evoked by the square (Fig. 9.9B, top) set up a propagating cortical response to the subsequently-presented bar (see Movie 9.3, also available at http://www.weizmann.ac.il/brain/grinvald/html/movie_gallery.html, Movies 12 and 13) that correlated with illusory motion because it was indistinguishable from cortical representations of real motion in this area. These findings emphasize the effect of spatiotemporal patterns of subthreshold synaptic potentials on cortical processing and the shaping of perception.

9.4 SPONTANEOUS CORTICAL ACTIVITY

Another series of studies was aimed at uncovering the principles underlying cortical activity in the absence of sensory stimulation, both that of single cells and that of the neuronal population.

9.4.1 On-Going Coherent Activity is Large and Accounts for the Variability of Evoked Responses

Hebb suggested that neurons operate in assemblies – networks of neurons, local or widespread, that communicate coherently to perform the computations required for various behavioral tasks (Hebb 1949). A significant contribution of VSDI has been the visualization of the dynamics of coherent neuronal assemblies, i.e., neuronal assemblies in which the activity of cells is time-locked, across the entire imaged area. The firing of a single neuron, recorded with an extracellular electrode, is used as a time reference for spike-triggered averaging of the VSD signal of each imaged pixel. With a sufficient number of spikes, any neuronal activity not time-locked to the reference neuron is averaged out, enabling selective visualization of those cortical locations in which activity

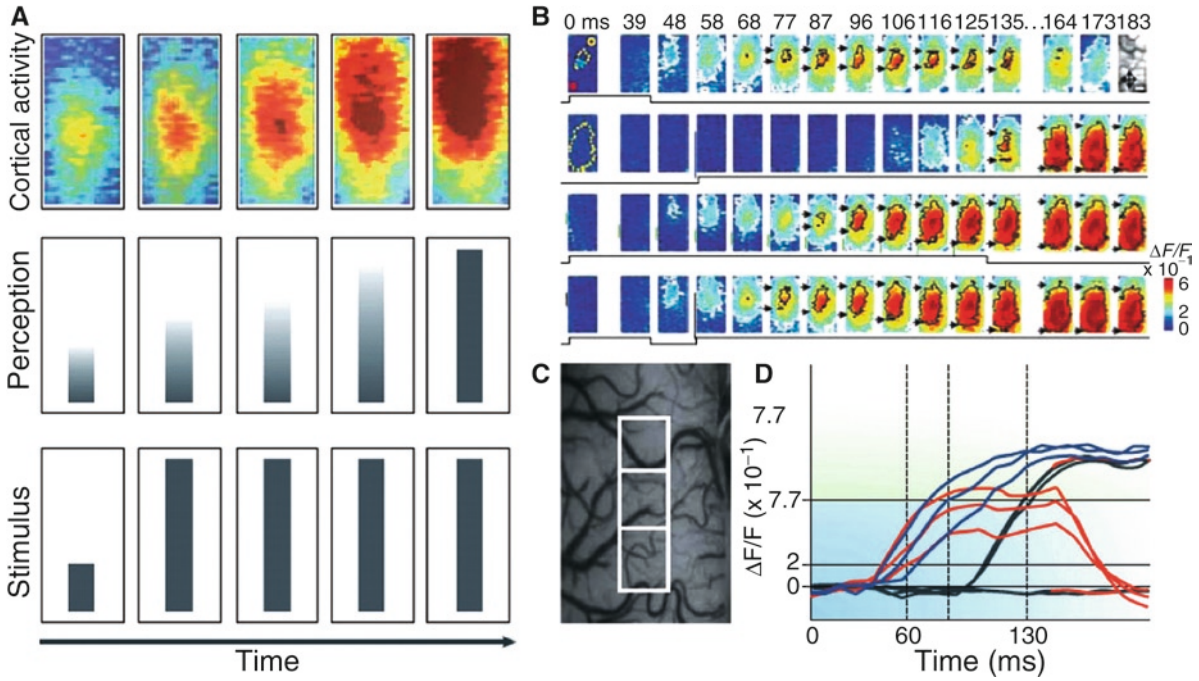

FIGURE 9.9. Priming by subthreshold spread of synaptic potential can account for the illusion of motion. (A) The line-motion stimulus (*bottom*), the perceived stimulus (*middle*) and the evoked cortical activity (*top*) over time. (B) Time series of the cortical representations of (from *top to bottom*) the stationary square and bars alone, the small moving square and the line-motion stimulus. *Yellow dotted contours* shown at 0 ms approximate the retinotopic representation of the stimuli; white contours delimit low-amplitude activity ($p < 0.05$). *Colored vertical lines* shown to the left of individual panels after stimulus onset indicate estimated sizes (or trajectory) of the stimuli along a posterior–anterior axis. Time in milliseconds after stimulus onset is indicated at the *top*. The time courses of stimulation are outlined at the bottom of each row. (C) The cortical area imaged with three contiguous regions of interest (ROIs, *white squares*) from which the time courses of responses shown in (D) were derived. (D) Responses to the small square (*red*), the line-motion condition (delayed bar after the *square*; *blue*) and *identical flashed bar* alone (*black*) within the three ROIs shown in (C). Note the large effect of the priming by the square on the latency of the response to the flashed bar (*blue traces* compared with *black traces*). Adapted from Jancke et al. (2004) with permission from Nature Publishing Group.

consistently occurred coherently with the firing of the reference neuron. A series of studies in anesthetized cat visual cortex explored the relationship of coherent spontaneous cortical states to evoked stimulus responses and to single-cell spikes.

An early surprising finding was that the amplitude of coherent, spontaneous, ongoing activity in neuronal assemblies was over half the amplitude of evoked activity. This suggested that spontaneous fluctuations in assembly activity affects evoked responses to sensory stimuli.

Indeed, while non-averaged evoked responses display a high degree of variability, this variability can be accounted for by the spatiotemporal patterns of ongoing activity (Fig. 9.10). The variable single-trial evoked response is well-predicted by summing the average evoked response (averaged over many stimulus presentations; Fig. 9.10A top) with the ongoing activity immediately preceding stimulus onset (the initial state), provided that for the duration of the response the ongoing state of the assembly remains similar to the initial state. This result suggests that ongoing activity is not merely "noise" and may provide the neuronal substrate for the dependence of sensory information processing on context, attention, behavioral and consciousness states, memory retrieval, etc.

9.4.2 Spontaneous Cortical States Are Internal Representations of Visual Attributes

A subsequent study explored the relationship between the spatial pattern of population activity coherent with a single neuron's spikes during spontaneous and evoked activity (Fig. 9.11). They were found to be very similar (see Movie 9.4). Furthermore, the instantaneous firing rate of a spontaneously active single neuron strongly depends on the spatial pattern of ongoing population activity in a large cortical area. During spontaneous activity, whenever the instantaneous spatial population pattern correlated highly with the spatial population pattern evoked by the preferred stimulus of the recorded neuron (Fig. 9.12A), its firing rate increased (Fig. 9.12C). Compared to the zero-centered distribution of correlation coefficients between each instantaneous recorded frame and the evoked orientation map (Fig. 9.12B), correlation coefficients during spikes had a strong bias towards positive values (Fig. 9.12D, and normalized in Fig. 9.12F). Strikingly, the dependence of single neurons' spiking on the global spontaneous activity is strong enough to allow reconstruction of the instantaneous spontaneous activity of single neurons (Fig. 9.12E).

In addition to revealing network influences in spontaneous spiking activity of individual neurons, the latest improvements in VSDI enabled exploration of spontaneous population dynamics and their relation to internal representations of sensory attributes. Ongoing activity in the visual cortex of the anesthetized cat was shown to be comprised of dynamically switching intrinsic cortical states, many of which closely correspond to orientation maps (Fig. 9.13). Cortical states that correspond to each and all orientations emerge spontaneously. When such an orientation state emerged spontaneously, it spanned several cortical hypercolumns and was usually followed by a state corresponding to a proximal orientation, or dissolved into an unrecognized state or noisy pattern after a few tens of milliseconds (see Movie 9.5, also available at http://www.weizmann.ac.il/brain/grinvald/html/movie_gallery.html, Movie 11).

Such dynamically switching cortical states could reflect the brain's internal context. Exploring cortical states is likely to reveal

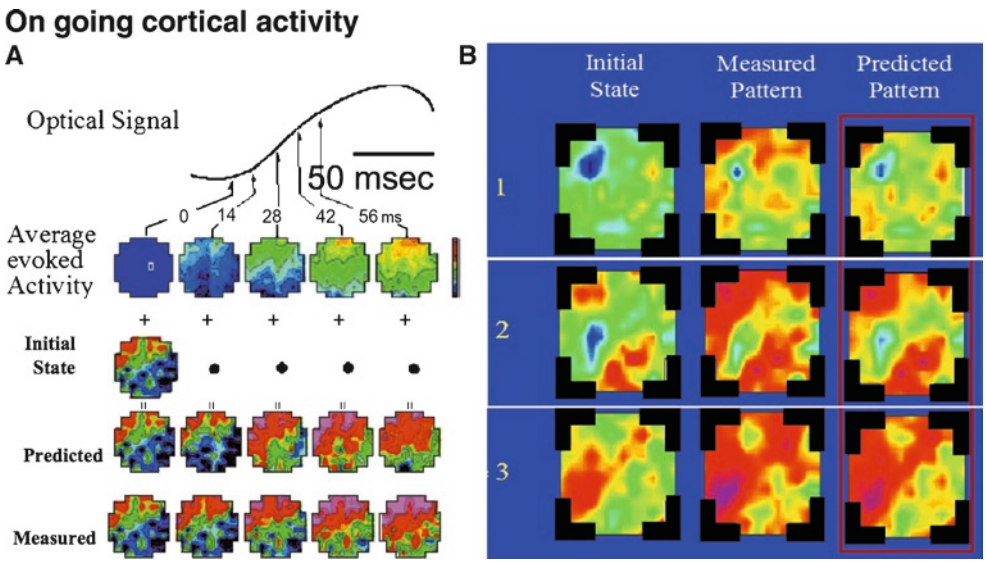

FIGURE 9.10. The impact of on-going activity: predicting cortical evoked responses in spite of their large variability. (A) In spite of the large variability of the evoked response, it can be predicted as a linear combination of the fixed pattern of an evoked response, and the instantaneous, constantly varying on-going activity pattern. Both patterns can be measured. The top trace shows the evoked response after averaging dozens of evoked trials to remove the variability. The average series of temporal patterns of the developing evoked response is shown in the *upper row* of frames. The *second row* shows the instantaneous on-going pattern which is assumed to be changing rather slowly and therefore assumed fixed for <50 ms. It is thus approximated by the initial state, i.e., the on-going pattern just prior to the onset of the evoked response. The *third row* (Predicted) shows the sum of the pattern of the initial state and the temporal sequence of the averaged pattern of evoked activity. The *bottom row* (Measured) shows that this predicted response and the measured response are very similar. (B) Three examples of comparing predicted and measured responses are shown. The predicted response was calculated as shown in (A). *Left columns*: Three very different Initial states. *Middle column*: Measured responses. *Right columns*: Predicted responses, obtained by adding the initial state in each case. Modified from Arieli et al. (1996).

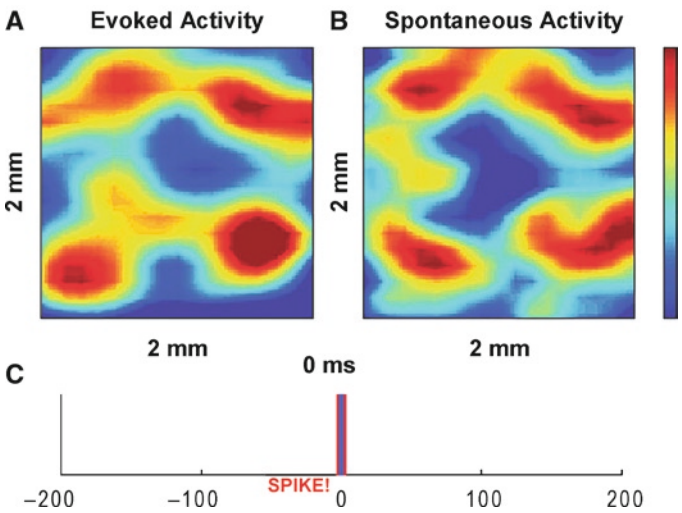

FIGURE 9.11. The preferred cortical state of a reference tuned neuron is similar to the related global functional architecture. (A) Orientation map of a 2-mm neighbourhood of the recorded neuron. This map represents the orientation-selective functional architecture of this neuron's environment. (B) The cortical state corresponding to spontaneous action potentials obtained by spike-triggered averaging of the spontaneous activity. The two patterns are nearly identical at the time of action potential occurrence. (C) The timing of the spike. In panel (A, B) it is stationary at time 0. In Movie 9.4 the spike shows the time of the average dynamics of the cortical state and the evoked activity. This result suggests that a neuron tends to fire spontaneously whenever a pattern corresponding to its parent functional architecture appears spontaneously.

new fundamental principles about neural strategies for cortical processing, representations of objects, memories, context, expectations, and particularly about the interplay between internal cortical representations and the sensory input in primary sensory areas.

9.4.3 Ongoing Activity in Anesthetized Monkeys

The previous studies using VSDI were carried out on anesthetized cats (Grinvald et al. 1989; Arieli et al. 1995, 1996; Tsodyks et al. 1999; Kenet et al. 2003; Ringach 2003). This has raised the question whether these results are relevant to behavior. Therefore, Omer and Grinvald (2004) and Omer and Rom (2008) performed VSDI of ongoing cortical activity in the visual cortices of awake monkeys simultaneously with measurements of single unit activity and the local-field potential. Coherent activity was found; however distinct cortical states reminiscent of orientation maps have so far remained undetectable. To rule out species difference Omer and his colleagues explored the anesthetized monkey, where the results were found to be similar to those in anesthetized cat. However, in the anesthetized monkey the spontaneous cortical activity shows a larger repertoire of cortical states; not surprisingly the two orthogonal OD maps were also spontaneously represented (Fig. 9.14), and to a larger extent than that of orientation.

Similarly, spike-triggered averaging (STA) using a sharply monocular reference neuron revealed a spatial pattern essentially identical to the evoked OD map (Fig. 9.15). It was noted that often both the orientation map and the OD map appeared spontaneously only on a small cortical area, unlike the findings in cat (Fig. 9.12) when the spontaneous pattern covered the entire imaged area.

9.5 OUTLOOK

Several groups, including those of Waggoner (Waggoner and Grinvald 1977; Waggoner 1979), Loew (Loew 1987) and Fromherz (Kuhn and Fromherz 2003), as well as our own, have made significant progress in developing VSDI during the last three decades by designing and synthesizing of new VSDs (Chap. 2). This chapter suggests that the technique has matured for shedding new light on

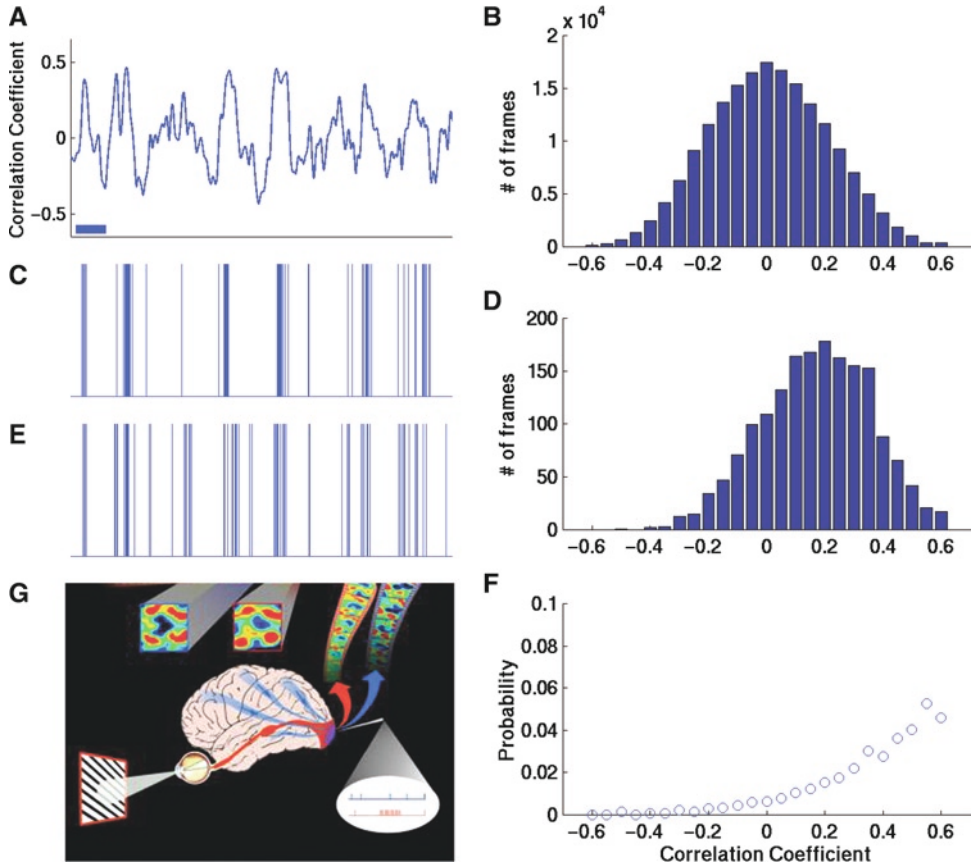

FIGURE 9.12. A spontaneous spike train of a single neuron can be predicted from the similarity of the instantaneous population activity pattern to the functional architecture. (A) The correlation coefficient between the instantaneous snapshot of population activity and the relevant functional architecture. (B) Histogram of the correlation coefficient for 20,480 frames. (C) The observed spike train: a strong upswing in the values of the similarity index is seen in panel (A) each time the neuron emits a burst of action potentials. Every strong burst is followed by a marked downswing in the values of the correlation coefficient. (D) Histogram of correlation coefficients for 338 frames during spike occurrences is highly skewed towards larger values. (E) Predicted instantaneous firing rate of a neuron, determined from the instantaneous similarity index, showing marked similarity to the bursting features in the observed spike train. (F) Same as (D), but normalized to the entire distribution shown in (B). (G) Dynamic brain activity in a given region is a combination of spontaneous internal activity in many cortical areas (blue stream) and the evoked responses (red). The spatial pattern that corresponds to spontaneous action potentials (blue frame) obtained by spike-triggered averaging and the evoked activity (red frame) are nearly identical. Adapted from Tsodyks et al. (1999) with permission from the American Association for the Advancement of Science.

neocortical function. Nevertheless, the signal-to-noise ratio that can be obtained with dyes, and the photodynamic damage they can cause, are limiting factors for yet better VSDI. Furthermore, different preparations often require dyes with different properties (Ross and Reichardt 1979; Cohen and Lesher 1986; Grinvald et al. 1988). Even different cortical areas in the same species can require different dyes (for example, one dye provided a high-quality signal in the rat somatosensory cortex but not in the rat olfactory bulb, although the bulb was well stained (Spors and Grinvald 2002)). Therefore, continuing efforts to make better dyes and new biophysical and optical innovations are important. Similarly, the development of new genetically engineered in vivo probes (Miyawaki et al. 1997; Siegel and Isacoff 1997; see also Chap. 14) will make experiments easier and improve the results. Of particular importance are probes that will stain only specific cell types and/or specific cellular compartments (axons, somata or dendrites).

Additional technological developments using multi-photon imaging, adaptive optics or other optical innovations to achieve three-dimensional imaging are desirable (for example, using special lenses that offer a shallow field of view; Rector et al. 1999). The combination of existing VSD probes with fluorescence resonance energy transfer (FRET) to detect electrical activity is also promising (Cacciatore et al. 1999). Similarly, excitation at the red edge of existing VSDs has been shown to provide up to ten-fold larger fractional change in the VSD signal size (Kuhn and Fromherz 2003; Kuhn et al. 2004), and imaging at the second harmonic frequency of new VSDs (Millard et al. 2003; Nemet et al. 2004) might also provide larger signals, enhancing the signal-to-noise ratio. The amount and nature of the data that have been and will be accumulated necessitate further methods of analysis, modeling and theoretical research that should lead to new conceptual frameworks regarding cortical function.

To increase the scope of meaningful neurophysiological data obtained from the same patch of cortex, VSDI should be combined with targeted-tracer injections, retrograde labeling, microstimulation and intracellular and extracellular recording. VSDI combined with electrical recordings enables neuroscientists to obtain information about spatiotemporal patterns of activity in coherent neuronal assemblies in the neocortex, at sub-columnar resolution. At present, no alternative imaging technique for visualizing organization and function in vivo provides a comparable spatial and temporal resolution. This level of resolution allows us to

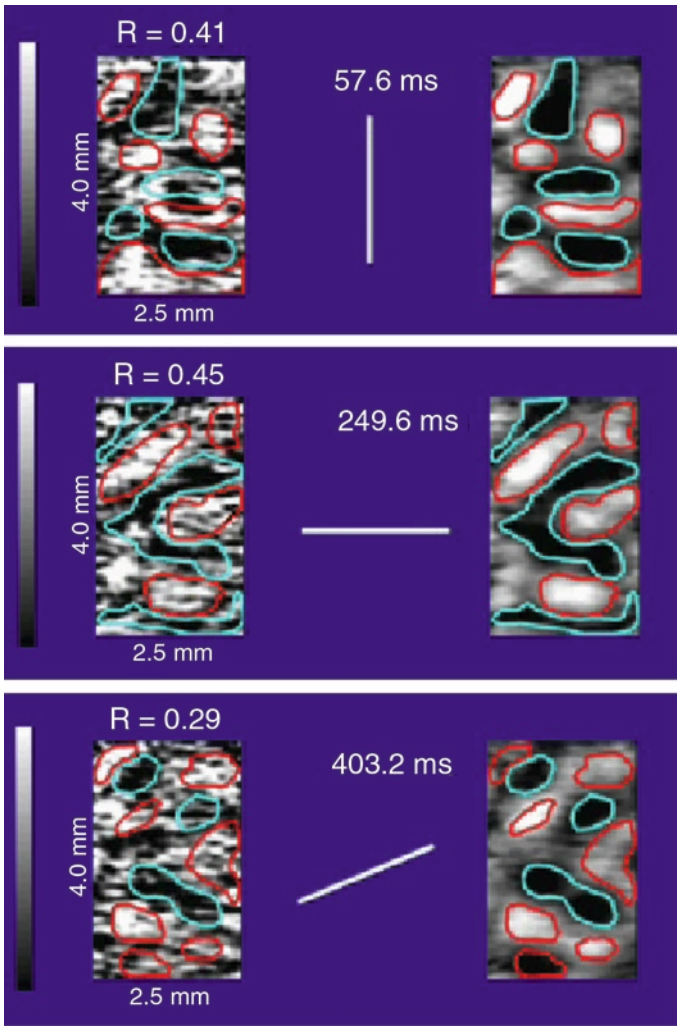

FIGURE 9.13. Snapshot of the spontaneous appearance of orientation representations – orientation maps. The three panels compare instantaneous patterns of spontaneous (*left side*) and evoked activity to the averaged functional map (*right side*). The orientation maps were obtained from responses to full-field gratings (at the orientation indicated in the middle). The maps on the left are 10msec snapshots of spontaneously appearing patterns; i.e., a single frame from a spontaneous recording session. *R* is the correlation value between the cortical representation of a given orientation and the snapshot. The number at the middle, top, denotes the time after recording onset at which the instantaneous pattern appeared.

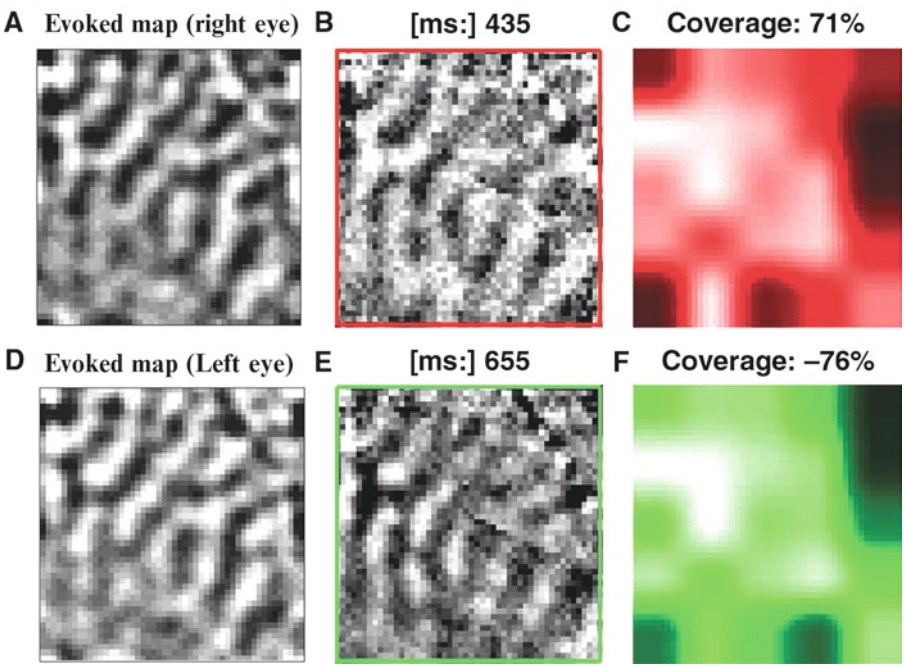

FIGURE 9.14. Spontaneous appearance of OD maps in anesthetized monkey. (A) OD map obtained by signal averaging of alternating stimulation of the right eye and the left eye each of them separately. (B) Snapshot of the spontaneous appearance of right eye map at 435 ms after the imaging onset. (**C**) The spontaneous map in (B) is highly correlated with the OD map in (A) in the red-white region the coverage was 71%. During the session the coverage of the cortical area with a functional map varied from 0 to ~80%. (D) The reversed differential OD map. (E) Snapshot of the spontaneous map for the contralateral eye. (F) Coverage in green for the contralateral eye. Similar maps were observed spontaneously also for orientation. Note the excellent signal-to-noise ratio for the 10 ms snap shot seen without any signal averaging.

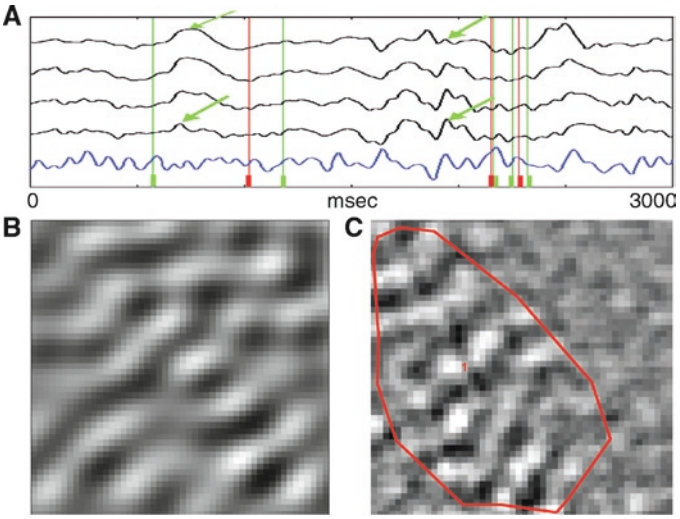

FIGURE 9.15. Spike-triggered averaging of spontaneous firing reveals that the cell fired when the entire population looked like its parent functional architecture. (A) 3 s of an imaging session. The top four traces are optical signals from 4 pixels out of 1,000,000 showing mostly slow waves. The simultaneously recorded spikes and the local field potential (LFP) are shown in blue. The red bars show the timing of single unit activity detected by the same electrode. (B) OD map obtained by differential imaging and signal averaging. (C) The same map was obtained by spike-triggered averaging of a single cell (red "1" in the center). The spatial pattern enclosed by the red contour exhibits a spatial pattern that corresponds to the OD map shown in (B). Note that the map has not spread to the entire imaged region.

address questions of both *where* and *when* processing takes place, providing great promise that this technique, integrated with other approaches, will contribute to the study of *how* processing occurs.

9.6 CONCLUSION

With the advent of the latest generation of VSDs and imaging equipment, a new era of exploration of cortical dynamics has ushered in. New-generation VSDI studies in cat and monkey visual cortex have revealed intricate spatiotemporal activity patterns underlying a variety of perceptual phenomena, underscoring the importance of large-scale subthreshold population responses and spontaneous states.

REFERENCES

Arieli A, Shoham D, Hildesheim R, Grinvald A (1995) Coherent spatio-temporal pattern of on-going activity revealed by real time optical imaging coupled with single unit recording in the cat visual cortex. J Neurophysiol 73: 2072–2093.

Arieli A, Sterkin A, Grinvald A, Aertsen A (1996) Dynamics of ongoing activity: explanation of the large variability in evoked cortical responses. Science 273:1868–1871.

Arieli A, Grinvald A (2002) Combined optical imaging and targeted electrophysiological manipulations in anesthetized and behaving animals. J Neurosci Methods 116:15–28.

Arieli A, Grinvald A, Slovin H (2002) Dural substitute for longterm imaging of cortical activity in behaving monkeys and its clinical implications. J Neurosci Methods 114:119–133.

Berger T, Borgdorff AJ et al. (2007) Combined voltage and calcium epifluorescence imaging in vitro and in vivo reveals subthreshold and suprathreshold dynamics of mouse barrel cortex. J Neurophysiol 97:3751–3762.

Bringuier V, Chavane F, Glaeser L, Frégnac Y (1998) Horizontal propagation of visual activity in the synaptic integration field of area 17 neurons. Science 283:695–699.

Cacciatore TW, Brodfuehrer PD et al. (1999) Identification of neural circuits by imaging coherent electrical activity with FRET-based dyes. Neuron 23:449–459.

Chavane F, Sharon D et al. (2010) Long-range horizontal spread of orientation selectivity in V1 is controlled by intracortical cooperatively. Submitted.

Cohen LB, Lesher S (1986) Optical monitoring of membrane potential:methods of multisite optical measurement. Soc Gen Physiol Ser 40:71–99.

Ferezou I, Bolea S, Petersen CCH (2006) Visualizing the cortical representation of whisker touch: voltage-sensitive dye imaging in freely moving mice. Neuron 50:617–629.

Ferezou I, Haiss F et al. (2007) Spatiotemporal dynamics of cortical sensorimotor integration in behaving mice. Neuron 56:907–923.

Grinvald A, Anglister L, Freeman JA, Hildesheim R, Manker A (1984) Real-time optical imaging of naturally evoked electrical activity in intact frog brain. Nature 308:848–850.

Grinvald A, Frostig RD, Lieke E, Hildesheim R (1988) Optical imaging of neuronal activity. Physiol Rev 68:1285–1366.

Grinvald A, Frostig RD et al. (1989) Optical Imaging of Activity in the Visual Cortex. In Lam D, Glibert CD (eds), MIT Press, Cambridge, USA.

Grinvald A, Lieke EE, Frostig RD, Hildesheim R (1994) Cortical point-spread function and long-range lateral interactions revealed by real-time optical imaging of macaque monkey primary visual cortex. J Neurosci 14:2545–2568.

Grinvald A, Shoham D et al. (1999) In-vivo optical imaging of cortical architecture and dynamics. In Windhorst U, Johansson H (eds) Modern techniques in neuroscience research. Springer, New York.

Grinvald A, Hildesheim R (2004) VSDI: a new era in functional imaging of cortical dynamics. Nat Rev Neurosci 5:874–885.

Hebb DO (1949) The organization of behavior. Wiley, New York.

Hubel DH, Wiesel TN (1962) Receptive fields, binocular interactions and functional architecture in the cat's visual cortex. J Physiol 160:106–154.

Jancke D, Chavane F, Grinvald A (2004) Imaging cortical correlates of a visual illusion. Nature 428:424–427.

Kenet T, Bibitchkov D, Tsodyks M, Grinvald A, Arieli A (2003) Spontaneously occurring cortical representations of visual attributes. Nature 425: 954–956.

Kuhn B, Fromherz P (2003) Anellated hemicyanine dyes in neuron membrane: molecular stark effect and optical voltage recording. J Phys Chem B 107:7903–7913.

Kuhn B, Fromherz P, Denk W (2004) High sensitivity of Stark-shift voltage-sensing dyes by one- or two-photon excitation near the red spectral edge. Biophys J 87:631–639.

Loew LM (1987) Optical measurement of electrical activity. CRC press, Boca Raton (FL), USA.

Millard AC, Jin L, Lewis A, Loew LM (2003) Direct measurement of the voltage sensitivity of second-harmonic generation from a membrane dye in patch-clamped cells. Opt Lett 28:1221–1223.

Miyawaki A, Llopis J et al. (1997) Fluorescent indicators for Ca^{2+} based on green fluorescent proteins and calmodulin. Nature 388:834–835.

Mountcastle VB (1957) Modality and topographic properties of single neurons of cat's somatic sensory cortex. J Neurophysiol 20:408–434.

Nemet BA, Nikolenko V, Yuste R (2004) Second harmonic imaging of membrane potential of neurons with retinal. J Biomed Opt 9:873–881.

Omer DB, Grinvald A (2004) The dynamics of evoked and ongoing activity in the behaving monkey. Rev Neurosci 19:S50.

Omer DB, Rom L, Grivald A (2008) The dynamics of ongoing activity in awake and anesthetized monkey are significantly different. Soc. Neurosci. USA, Book of Abstracts.

Orbach HS, Cohen LB (1983) Simultaneous optical monitoring of activity from many areas of the salamander olfactory bulb. A new method for studying functional organization in the vertebrate CNS. J Neurosci 3: 2251–2262.

Orbach HS, Cohen LB, Grinvald A (1985) Optical mapping of electrical activity in rat somatosensory and visual cortex. J Neurosci 5:1886–1895.

Petersen CCH, Grinvald A, Sakmann B (2003a) Spatiotemporal dynamics of sensory responses in layer 2/3 of rat barrel cortex measured in vivo by

voltage-sensitive dye imaging combined with whole-cell voltage recordings and neuron reconstructions. J Neurosci 23:1298–1309.

Petersen CCH, Hahn TTG, Mehta M, Grinvald A, Sakmann B (2003b) Interaction of sensory responses with spontaneous depolarization in layer 2/3 barrel cortex. Proc Natl Acad Sci U S A 100:13638–13643.

Ratzlaff EH, Grinvald A (1991) A tandem-lens epifluorescence macroscope: hundred-fold brightness advantage for wide-field imaging. J Neurosci Methods 36:127–137.

Rector DM, Rogers RF, George JS (1999) A focusing image probe for assessing neural activity in vivo. J Neurosci Methods 91:135–145.

Ringach DL (2003) Neuroscience: states of mind. Nature 425(6961):912–913.

Ross WN, Reichardt LF (1979) Species-specific effects on the optical signals of voltage sensitive dyes. J Membr Biol 48:343–356.

Salzberg BM, Davila HV, Cohen LB (1973) Optical recording of impulses in individual neurons of an invertebrate central nervous system. Nature 246:508–509.

Sharon D, Grinvald A (2002) Dynamics and constancy in cortical spatiotemporal patterns of orientation processing. Science 295:512–515.

Sharon D, Jancke D, Chavane F, Na'aman S, Grinvald A (2007) Cortical response field dynamics in cat visual cortex. Cereb Cortex 17:2866–2877.

Shoham D, Glaser DE et al. (1999) Imaging cortical dynamics at high spatial and temporal resolution with novel blue voltage-sensitive dyes. Neuron 24:791–802.

Siegel MS, Isacoff EY (1997) A genetically encoded optical probe of membrane voltage. Neuron 19:735–741.

Spors H, Grinvald A (2002) Temporal dynamics of odor representations and coding by the mammalian olfactory bulb. Neuron 34:1–20.

Sterkin A, Lampl I, Ferster D, Grinvald A, Arieli A (1998) Real time optical imaging in cat visual cortex exhibits high similarity to intracellular activity. Neurosci Lett 51:S41.

Tasaki I, Watanabe A, Sandlin R, Carnay L (1968) Changes in fluorescence, turbidity, and birefringence associated with nerve excitation. Proc Natl Acad Sci U S A 61:883–888.

Tsodyks M, Kenet T, Grinvald A, Arieli A (1999) The spontaneous activity of single cortical neurons depends on the underlying global functional architecture. Science 286:1943–1946.

Waggoner AS, Grinvald A (1977). Mechanisms of rapid optical changes of potential sensitive dyes. Ann N Y Acad Sci 303:217–241.

Waggoner AS (1979) Dye indicators of membrane potential. Annu Rev Biophys Bioeng 8:47–63.